Surface modifications with Lissajous trajectories using atomic force microscopy

Wei Cai and Nan Yao[a)]
Princeton Institute for Science and Technology of Materials, Princeton University, Princeton, New Jersey 08544, USA

(Received 26 June 2015; accepted 22 August 2015; published online 15 September 2015)

In this paper, we report a method for atomic force microscopy surface modifications with single-tone and multiple-resolution Lissajous trajectories. The tip mechanical scratching experiments with two series of Lissajous trajectories were carried out on monolayer films. The scratching processes with two scan methods have been illustrated. As an application, the tip-based triboelectrification phenomenon on the silicon dioxide surface with Lissajous trajectories was investigated. The triboelectric charges generated within the tip rubbed area on the surface were characterized *in-situ* by scanning Kelvin force microscopy. This method would provide a promising and cost-effective approach for surface modifications and nanofabrication. © *2015 AIP Publishing LLC*.
[http://dx.doi.org/10.1063/1.4931087]

Atomic force microscopy (AFM) nanofabrication is a flexible and low-cost method for the preparation of nanoscale structures on the surface of various kinds of materials. Depending on different types of AFM tips, a lot of tip-sample interactions can be utilized for material surface modifications, including mechanical, electrical, chemical, and thermal effects.[1–5] Due to the inherent nature of the scanning probe microscope (SPM),[6] raster scan patterns are required for both imaging and nanofabrication. Structures consisting of lines on the surface can be fabricated by raster scan patterns.[2] For complex or irregular patterns, vector-scan controlled nanolithography has been proposed to move the tip along a desired path.[7,8] But the fabrication speed was limited to several nanometers per second. Enhanced raster scan patterns were proposed by a rotating-tip-based technique[9] or in-plane circular vibration method.[10] In these methods, during the fabrication processes, the tip did circular motions, which were helpful in increasing the lithographic throughput.

Recently, in AFM imaging methods, several novel non-raster scan trajectories have been proposed, such as spiral,[11] cycloid,[12] and Lissajous patterns.[13–15] One thing these scan patterns have in common is that the drive signals in x and y axes are all single-tone waveforms. So the advantage of these scan trajectories is that the scan speed can be increased without exciting the traditional scanner's oscillation at higher-order harmonics.[16–18] Among these scan trajectories, spiral and cycloid-like patterns can be used to cover a round shape and a capsule shaped area, respectively. Only Lissajous trajectory can map a square area. And the corresponding scan shape, the density of the scan path, and the scan time can be regulated by the small frequency difference between the two axes of the scanner.[15] However, the scan method involving Lissajous trajectories for nanofabrication has not been reported yet.

In this article, first, we present the methods to calculate the Lissajous scan trajectories for AFM surface modifications based on single-tone waveforms and multiple-frequency waveforms theoretically. Then, as demonstrations, the experiments on the tip mechanical scratching method with two kinds of Lissajous trajectories were carried out. As an application, the triboelectrification phenomenon induced by a scanning AFM tip on silicon dioxide surface[19] with Lissajous trajectories was investigated. The triboelectric charges accumulated within the tip rubbed area on the surface were characterized *in-situ* by using the scanning Kelvin probe force microscopy (SKPM). This method would provide a promising and cost-effective approach for surface modifications and nanofabrication.

To develop Lissajous trajectories used for AFM nanofabrication, inspired by the work of Bazaei *et al.*[15] and Yong *et al.*,[14] trajectories can be expressed by two single-tone cosine waveforms as shown in Equation (1). The phase values of the waveforms are set to zero. A_x and A_y represent the half scan range in x- and y-axis, respectively. x_0 and y_0 are the scan offset. There is a small difference between the two frequencies f_x and f_y. Typically assuming $f_x > f_y$, the ratio of the frequencies f_x/f_y, which is rational, can be expressed by Equation (2), where N is a natural number for the ratio control. The value of N is inversely proportional to the frequency difference. The shape of the Lissajous trajectory is highly sensitive to the frequency ratio; thus, the pattern can be designed by choosing different values of N. If N is large enough, the Lissajous trajectories can cover the whole rectangular area with the size of $2A_x$ by $2A_y$

$$X = x_0 + A_x \cos(2\pi f_x t), \quad Y = y_0 + A_y \cos(2\pi f_y t), \tag{1}$$

$$\frac{f_x}{f_y} = \frac{2N}{2N-1}. \tag{2}$$

Following the design steps proposed by Yong *et al.*, the trajectory can be calculated as follows.[14] First, the target resolution of Lissajous trajectory h is defined by the distance between the two nearest cross points around the origin. When N is a large number and assuming that $A_x = A_y = A$, then N can be determined by using Equation (3)[15]

[a)]Author to whom correspondence should be addressed. Electronic mail: nyao@princeton.edu.

 © 2015 AIP Publishing LLC

$$N \approx \left[\frac{\pi}{\sqrt{2}}\frac{A}{h}\right]. \quad (3)$$

In this situation, if f_x is known, then the f_y can be determined by Equation (2). Finally, after setting the offsets x_0 and y_0, the trajectory can be determined by Equation (1) and the period of the trajectory can be expressed by Equation (4).

$$T = \frac{1}{|f_x - f_y|} = \frac{2N}{f_x}. \quad (4)$$

It is worth noticing that only with a half-period of Lissajous trajectory, the squared area can be fully scanned.[15] So, in our experiments, one scan method is implemented by directly using a half-period of the designed Lissajous trajectory. The other scan method which can be used in nanofabrication is based on the multiple-resolution Lissajous scanning.[13] In this method, the frequency (e.g., f_y) is not fixed during the scan period, as shown in Equation (5). The whole scan time can be divided into M parts. For every value of M, except for the first part, the time duration is a half-period Lissajous trajectory with a period of T_m, as shown in Equation (6). The corresponding frequency $f_{y,m}$ can be expressed by Equation (7), where Δf is the minimum difference of two frequencies ($\Delta f = f_x - f_{y,M}$). Phase shift φ_m in every part of trajectories, which is given by Equation (8), is necessary to ensure Y_m is continuous

$$Y_m = y_0 + A_y \cos(2\pi f_{y,m} t + \varphi_m), \quad (5)$$

$$T_m = \frac{1}{2^{M-m}} T, \quad m = 1, 2, 3..., M, \quad (6)$$

$$f_{y,m} = f_x - 2^{M-m}\Delta f, \quad m = 1, 2, 3..., M, \quad (7)$$

$$\varphi_m = (M - m)\pi, \quad m = 1, 2, 3..., M. \quad (8)$$

Figs. 1(a)–1(c) give the schematics of the designed Lissajous trajectories by the single-tone method with different time durations, which are [0, T/4], [T/4, T/2], and [0, T], respectively. In experiments, the target resolution $h = 80$ nm and the half scan range $A = 1$ μm were used in generated Lissajous trajectories. The driving frequencies were $f_x = 1$ Hz and $f_y = 0.982$ Hz; therefore, the corresponding $N = 28$. Figs. 1(d)–1(f) show an example with multi-resolution method with $M = 4$ in calculations and experiments. Keeping the maximum target resolution, the scan range and the x frequency are the same as the former parameters. The y frequency and the phase in the corresponding time intervals were changed. The y frequency was varied as $f_y = 0.857$ Hz, 0.929 Hz, and 0.964 Hz, respectively. And the y phase as $\varphi = 3\pi$, 2π, and π. A_x and A_y were used to control the size and the aspect ratio of the Lissajous scan area. The amplitude values depend on the scanner's lateral coefficient ($\alpha \approx 306$ nm/V on our instrument). So, the corresponding amplitude $A_x = A_y$ in volts were at ~3.27 V. Fig. 1(d) is a full period of Lissajous trajectory with $T_1 = T/8$. Figs. 1(e) and 1(f) are a half period of Lissajous trajectory with $T_2 = T/4$ and $T_3 = T/2$, respectively.

To illustrate our methods, AFM surface modifications and characterization were carried out under ambient conditions by using a Veeco Dimension V AFM with Nanoscope V Controller. Standard tapping mode silicon cantilevers (RTESP) were used for mechanical scratching. Before the experiments, the deflection sensitivity and the spring constant of the cantilevers were calibrated by using the force distance curves and the thermal tune method,[20] respectively. For sample preparations, we performed a surface treatment to ideally form a monolayer of C_{18} chains on a clean Si/SiO_2 substrate for scratching tests. The thickness of the film is ~5 nm, and the average surface roughness measured is ~2.5 nm. For tip triboelectrification experiments, PtIr coated cantilevers (NSG03/Pt, NT-MDT, nominal spring constant $k = 1.74$ N/m, and resonance frequency $f_0 = 90$ kHz) were used. The accumulated surface charges were characterized by SKPM.[21] All AFM images were post-processed using Gwyddion software.[22]

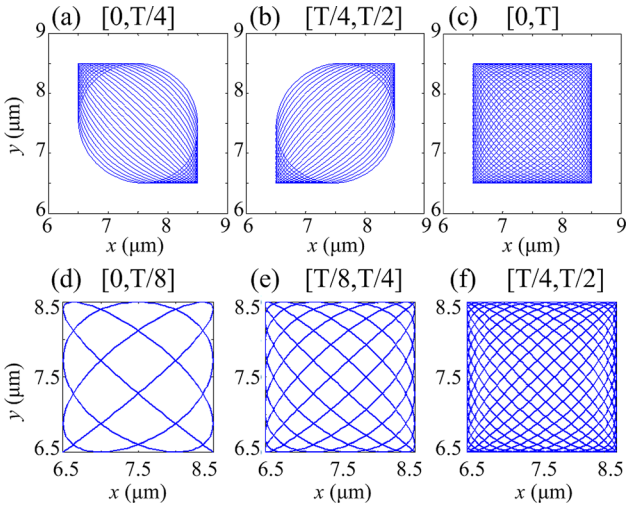

FIG. 1. Scan methods used for AFM nanofabrication with Lissajous trajectories. (a)–(c) Trajectories with different period of time. The length of the period are [0, T/4], [T/4, T/2], and [0, T], respectively. For a whole period of the Lissajous pattern, the squared area would be scanned twice. (d)–(f) Another method of Lissajous trajectory with different frequency difference. The "preview" function would be provided by increasing the resolution of the time-lapse frames, if the requirement of the fabrication is satisfied, the fabrication processes will be stopped.

In the first experiment, the trajectory was prepared by a homemade program and imported into the SPM control software. The normal force applied on the tip was ~2 μN. Figs. 2(a)–2(c) are fabricated on the different positions of the sample surface with different time duration. In the first phase,

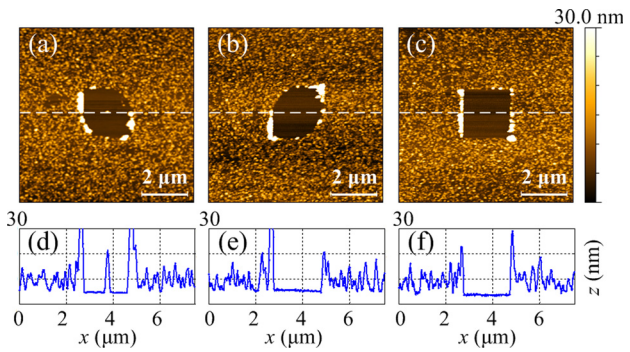

FIG. 2. The corresponding scratched surfaces (a)–(c) by using the Lissajous patterns shown in Figs. 1(a)–1(c). Figs. 2(d)–2(f) are the corresponding cross-section lines marked in Figs. 2(a)–2(c), respectively.

the first quartered period of Lissajous trajectory was used, as shown in Fig. 1(a). The tip started moving from the right bottom corner of the squared area to the left up corner, and the trajectory gradually became a circle. The materials on the substrate were removed/scratched by the scanning tip correspondingly, as shown in Fig. 2(a). In the second quartered period, as shown in Fig. 1(b), the trajectory evolves from a circle to a line and finally moves to the upper right corner of the square. The diagonally opposite corner was added in scan area, and the center round area was scanned again from different directions. The result of scratched surface is shown in Fig. 2(b). This method is advantageous as if there are some particles left in the center of the scratched area after finishing the first quartered period scan, in the second quartered period, most of the particles can be swept out by the tip. Fig. 1(c) shows a full period of Lissajous trajectory which can be seen as the overlap of Figs. 1(a) and 1(b) and then a repetition once in the opposite direction. Fig. 2(c) shows the corresponding square-shaped scratched surface with a full period of Lissajous trajectory. The monolayer film on the substrate has been removed. The fabrication time used for scratching elliptic-like patterns in Figs. 2(a) and 2(b) equals to a quarter of a period. According to Equation (4), the period of a whole trajectory equals to $T = 2N/f_x$, where $N = 28$ and $f_x = 1$ Hz in experiments. The fabrication time in Figs. 2(a) and 2(b) were ~14 s. In Fig. 2(c), the time used for scratching was ~56 s. Figs. 2(d)–2(f) are the corresponding cross-section lines marked in Figs. 2(a)–2(c), respectively.

In the second experiment, the multi-resolution Lissajous trajectories were used for surface modifications. The scan method was designed by following the idea of "preview" of the scanned area.[13] The normal force was set at the same value as in the first experiment. Figs. 3(a)–3(c) show the morphology of the scratched areas. To illustrate the fabrication processes, Fig. 3(a) shows the morphology of the scratched area with the trajectory as shown in Fig. 1(d). Fig. 3(b) shows the morphology scratched with the trajectories showed in Figs. 1(d) and 1(e). Fig. 3(c) shows the morphology scratched with the trajectories in Figs. 1(d)–1(f). From the scratched results, in the first period of the fabrication process ($T/8$), because the target resolution was too low, the scratched area could not be completely distinguished. Then, in the next period ($T/8$), the resolution of Lissajous pattern was increased. The scratched area could be seen, because the trajectory covered most of the squared area. But the resolution of the trajectory needed to be further improved since a lot of debris was present on the scratched surface. In the third period ($T/4$), because the resolution of Lissajous pattern was increased, most of the debris on the scratched area was swept to the border of the area. From these time-lapse frames, this function can be compared to the preview function in imaging experiments.[13] According to Equation (6), in Figs. 3(a)–3(c), the fabrication times were ~7 s, ~14 s, and ~28 s, respectively. Figs. 3(d)–3(f) are the corresponding cross-section lines marked in Figs. 3(a)–3(c), respectively.

As an application, we then carried out tip-based triboelectrification experiments with Lissajous patterns. The principle of nanoscale triboelectrification was proposed by Zhou *et al.*[19] By using a silicon AFM tip to contact a silicon dioxide surface, negative charges would be generated and accumulated on the rubbed surface during scanning. The surface potential generated by the charges can be characterized by SKPM. In experiments, for *in-situ* modification and characterization, a worn-out conductive AFM tip was used. So contacting the surface with silicon tip and sensing the electrostatic field can be simultaneously satisfied. For charge generation in contact mode, the trajectory we used is the same as in Fig. 1(c). The cantilever deflection sensitivity (~32.10 nm/V), the setpoint value (~0.2 V), and the force constant (~1.63 N/m) were calibrated before experiments. The normal force (~10 nN) was evaluated with Hook's law by multiplying these parameters. Two cycles of the Lissajous trajectory were performed with the fabrication time of ~112 s in charge generation that means the squared area was rubbed for four times. Then we switched to the SKPM mode for mapping the surface charges. The lift height was set to 50 nm. Fig. 4(a) gives the topographic image of the silicon dioxide surface after rubbing and Fig. 4(b) shows the corresponding surface potential mapping. From the surface potential mapping, the rubbed area shows a lower potential indicating that the negative triboelectric charges accumulated in this area. From the cross-section lines of the

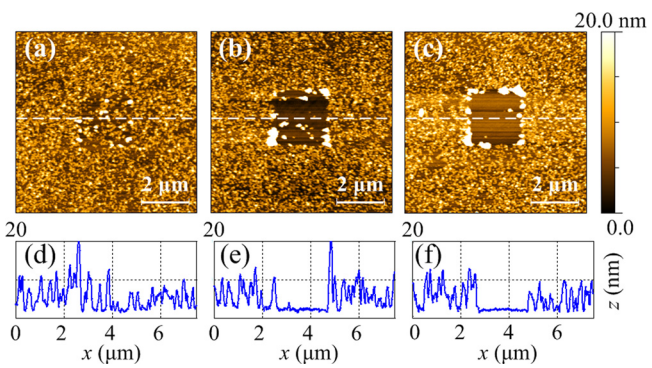

FIG. 3. Surface modifications (a)–(c) by the tip-scratching method with multi-resolution Lissajous patterns shown in Figs. 1(d)–1(f). The trajectories with low resolution were marked on the topographic images (a) and (b). Figs. 3(d)–3(f) are the corresponding cross-section lines marked in Figs. 3(a)–3(c), respectively.

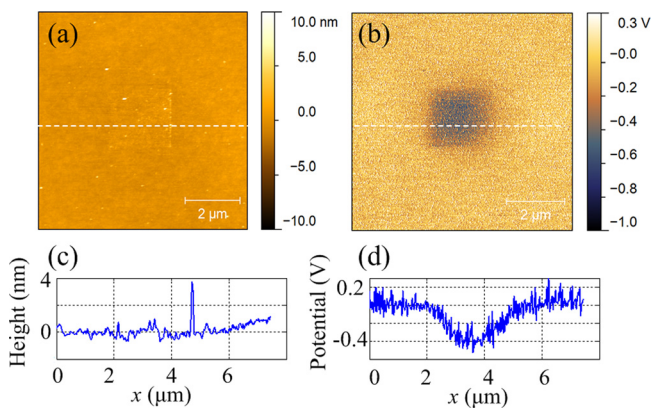

FIG. 4. Tip-based triboelectric charges generated with Lissajous trajectories. The topography image (a) and the surface potential mapping (b) of the surface captured after scanning with two periods of Lissajous trajectories. Figs. 4(c) and 4(d) are the corresponding cross-section lines marked in Figs. 4(a) and 4(b), respectively.

surface potential suggest that the rubbed area is $\sim$0.4 V lower than the surrounding areas.

Using Lissajous trajectories in surface modifications, the largest size of the patterns is only restricted within the AFM scanner's range in x- and y-axis ($\sim$90 μm in our microscope). In our experiments, the fabrication size is $\sim$2 μm and the highest frequency can achieve several tens of Hz with conventional PID (proportional integral derivative) feedback controller. So, the corresponding fabrication time per frame can be reduced from minutes to several seconds. But it appears there are other factors in nanofabrication which must be taken into account, e.g., if the scan rate is too high ($f_x \sim 10$ Hz) in mechanical scratching, it would result in large portions of the debris left on the scanned area. So, in the experiments, the x scan rate f_x was reduced to $\sim$1 Hz to decrease the debris caused by the tip-sample interactions. In the triboelectrification tests, the scan rate was also reduced to decrease the wear of the sample surface which caused by the friction between the tip and the sample.

In summary, we have analyzed single-tone and multiple-resolution methods for AFM nanofabrication with Lissajous trajectories. Then, the experiments on the tip mechanical scratching with two series of Lissajous trajectories were carried out on monolayer films. The fabrication processes in these two methods have been illustrated. As an application, tip-based triboelectrification phenomenon on SiO_2 surface with Lissajous trajectories was investigated. The triboelectric charges generated in the tip rubbed area on the surface were characterized *in-situ* by SKPM. This method would provide a promising and cost-effective approach for surface modifications and nanofabrication.

This work was also supported in part by the National Science Foundation-MRSEC program through the Princeton Center for Complex Materials (DMR-1420541).

[1]G. Ricardo, W. K. Armin, and R. Elisa, Nat. Nanotechnol. **9**(8), 577–587 (2014).
[2]A. A. Tseng, Small **7**(24), 3409–3427 (2011).
[3]B. Fabre and C. Herrier, RSC Adv. **2**(1), 168–175 (2012).
[4]K. Salaita, Y. Wang, and C. A. Mirkin, Nat. Nanotechnol. **2**(3), 145–155 (2007).
[5]D. Pires, J. L. Hedrick, A. D. Silva, J. Frommer, B. Gotsmann, H. Wolf, M. Despont, U. Duerig, and A. W. Knoll, Science **328**(5979), 732–735 (2010).
[6]A. Humphris, M. Miles, and J. Hobbs, Appl. Phys. Lett. **86**(3), 034106 (2005).
[7]U. Kunze and B. Klehn, Adv. Mater. **11**(17), 1473–1475 (1999).
[8]B. Klehn and U. Kunze, J. Appl. Phys. **85**(7), 3897–3903 (1999).
[9]B. A. Gozen and O. B. Ozdoganlar, Nanoscale Res. Lett. **5**(9), 1403–1407 (2010).
[10]L. Zhang and J. Dong, Nanotechnology **23**(8), 85303 (2012).
[11]I. Mahmood and S. R. Moheimani, Nanotechnology **20**(36), 365503 (2009).
[12]Y. Yong, S. Moheimani, and I. Petersen, Nanotechnology **21**(36), 365503 (2010).
[13]T. Tuma, J. Lygeros, V. Kartik, A. Sebastian, and A. Pantazi, Nanotechnology **23**(18), 185501 (2012).
[14]Y. K. Yong, A. Bazaei, and S. O. R. Moheimani, IEEE Trans. Nanotechnol. **13**(1), 85–93 (2014).
[15]A. Bazaei, Y. K. Yong, and S. R. Moheimani, Rev. Sci. Instrum. **83**(6), 063701 (2012).
[16]G. E. Fantner, G. Schitter, J. H. Kindt, T. Ivanov, K. Ivanova, R. Patel, N. Holten-Andersen, J. Adams, P. J. Thurner, and I. W. Rangelow, Ultramicroscopy **106**(8), 881–887 (2006).
[17]T. Ando, T. Uchihashi, and T. Fukuma, Prog. Surf. Sci. **83**(7–9), 337–437 (2008).
[18]B. P. Brown, L. Picco, M. J. Miles, and C. F. Faul, Small **9**(19), 3201–3211 (2013).
[19]Y. S. Zhou, Y. Liu, G. Zhu, Z.-H. Lin, C. Pan, Q. Jing, and Z. L. Wang, Nano Lett. **13**(6), 2771–2776 (2013).
[20]R. Levy and M. Maaloum, Nanotechnology **13**(1), 33 (2002).
[21]V. Palermo, M. Palma, and P. Samorì, Adv. Mater. **18**(2), 145–164 (2006).
[22]D. Nečas and P. Klapetek, Open Phys. **10**(1), 181–188 (2012).